

## Fluidization of granular media wetted by liquid $^4\text{He}$

K. Huang,<sup>\*</sup> M. Sohaili, M. Schröter, and S. Herminghaus<sup>†</sup>

*Max Planck Institute for Dynamics and Self-Organization, Bunsenstrasse 10, 37073 Göttingen, Germany*

(Received 17 October 2008; published 27 January 2009)

We explore experimentally the fluidization of vertically agitated polymethylmethacrylate spheres wetted by liquid  $^4\text{He}$ . By controlling the temperature around the  $\lambda$  point, we change the properties of the wetting liquid from a normal fluid (helium I) to a superfluid (helium II). For wetting by helium I, the critical acceleration for fluidization ( $\Gamma_c$ ) shows a steep increase close to the saturation of the vapor pressure in the sample cell. For helium II wetting,  $\Gamma_c$  starts to increase at about 75% saturation, indicating that capillary bridges are enhanced by the superflow of the unsaturated helium film. Above saturation,  $\Gamma_c$  enters a plateau regime where the capillary force between particles is independent of the bridge volume. The plateau value is found to vary with temperature and shows a peak at 2.1 K, which we attribute to the influence of the specific heat of liquid helium.

DOI: [10.1103/PhysRevE.79.010301](https://doi.org/10.1103/PhysRevE.79.010301)

PACS number(s): 45.70.-n, 68.08.Bc, 67.25.dm

It is a well-known experience that the addition of a certain amount of wetting liquid to a pile of sand increases its mechanical stability dramatically [1–5], leading to a material stiff enough for sculpting sand castles. The increased mechanical stability of wet granulates is due to the formation of liquid bridges between adjacent grains, which exert attractive forces by virtue of their surface tension [6–10]. As has recently been shown, the presence of liquid changes the acoustic properties of the granulate as well [11]. Wet granular media exist in many chemical, pharmaceutical, or food production processes, where the question how to handle them appropriately is of great economic significance [12–14]. Moreover, wet granular media are also model systems to study phase transitions far from equilibrium [15]. A detailed understanding of the interaction between the liquid and the grains is therefore of major importance.

In both basic research and many industrial processes, vertical vibration is a widely used fluidization scheme [16]. For wet granulates, an extra force must be exerted in wet grains to overcome the cohesive capillary forces, in contrast to the fluidization of a dry granular pile [17–20]. These forces increase the critical shaking acceleration  $\Gamma_c$  needed for fluidization, which makes  $\Gamma_c$  a good parameter to study the influence of a wetting liquid [21–23].

Here we measure  $\Gamma_c$  for polymethylmethacrylate spheres wetted by liquid helium. Helium wets most substrates perfectly [24–26] so that a zero contact angle can be assumed. When its temperature is below the  $\lambda$  point (2.17 K for bulk helium), liquid helium will undergo a phase transition into a superfluid (helium II) where many interesting phenomena such as the “fountain effect” arise, owing to its two-fluid properties [27–32]. In this paper we study how the difference between a superfluid and a normal fluid changes the mechanical properties of a granular medium wetted by this liquid.

A sketch of the experimental setup is shown in Fig. 1. The granular sample consists of 0.6 g polymethylmethacrylate spheres (Bangs Labs) with an average diameter of  $d$

$\approx 10 \mu\text{m}$  and 15% width of the size distribution. This prevents the formation of a crystalline packing which would result in unwanted side effects. The sample is fluidized by sinusoidal vertical vibrations with a driving frequency  $f = 110 \text{ Hz}$  and a nondimensional acceleration  $\Gamma = 4\pi^2 f^2 A / g$ , where  $g$  is the gravitational acceleration and  $A$  is the shaking amplitude. The sample is contained in a cylindrical cell made of 99.95% oxygen-free copper, which ensures good thermal contact with the surrounding helium bath. The temperature in the cryostat is controlled by adjusting the pressure above the liquid helium.

The amount of helium in the sample cell is controlled by adding room temperature helium gas, which was passed through a cold trap for purification. A well-defined amount of helium gas was admitted to the cell using a gauged cylinder volume. All measurements are taken after the pressure in the cell becomes stable.

The sample was illuminated with laser pulses with 532 nm wavelength and a repetition rate of 22 Hz, phase locked to the vibration of the sample. The speckle pattern from the back-scattered light is captured with a charge coupled device camera (Hamamatsu C9300) with a quantum efficiency 58% at this wavelength. A polarizer in front of the camera suppresses directly reflected light. The camera and laser are synchronized so that the images are taken at a fixed phase of every fifth vibration cycle. The power injected by the laser pulses is on the order of  $10^{-6} \text{ W}$ . This is at least one order of magnitude less than the energy injected by vibrations, which we estimate to be  $\approx 2.6 \times 10^{-5} \text{ W}$  from the inelastic collisions between the sample and the bottom plate at  $\Gamma = 2$ .

To create a reproducible initial packing, we first fully fluidize the sample by shaking it for a few seconds with a  $\Gamma$  of  $6 \pm 1$ . Then we ramp  $\Gamma$  down to below 1 during approximately 1 min. The critical acceleration for fluidization  $\Gamma_c$  is then measured by slowly increasing and decreasing  $\Gamma$ .  $\Gamma_c$  differs by maximally 15% for fluidization and solidification [23]; the values reported here are averages between both values. The transition between solid and fluid states of the sample is determined by visual inspection of the variation of the speckle pattern in real time. As soon as the sample fluidizes, the speckle pattern no longer stays stable and starts to

<sup>\*</sup>kai.huang@ds.mpg.de

<sup>†</sup>stephan.herminghaus@ds.mpg.de

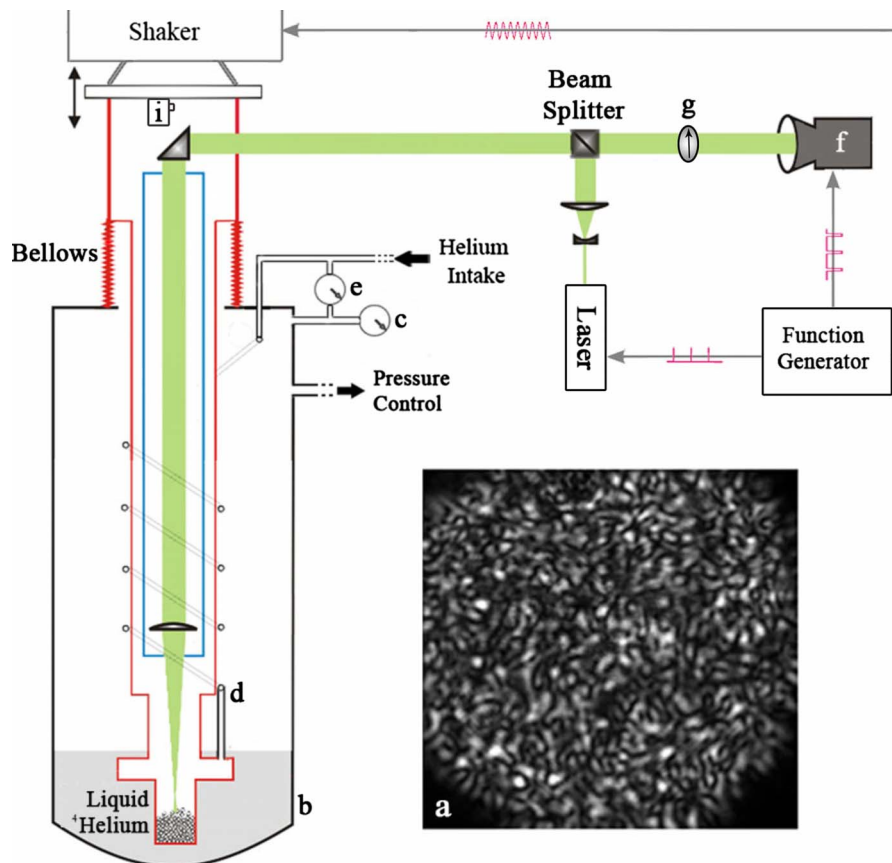


FIG. 1. (Color online) Sketch of the experimental setup. (a) is a typical top view of the sample. The temperature in the cryostat (b) is adjusted by controlling the pressure [measured by pressure gauge (c)] above the liquid helium. Helium gas is added into the sample chamber through a capillary (d). Gauge (e) measures the pressure difference between cell and cryostat. The sample is illuminated by laser pulses, and images are taken by a charge-coupled device camera (f) with a polarizer (g) in front. The sample cell can be vibrated vertically by an electrodynamic shaker (LDS V555) which is mounted upside down above the cryostat. The strength of vibration is measured by an accelerometer (PCB Piezotronics 353B33) (i).

vary with time. This method was found to agree with measurements based on the correlation of subsequent images.

Figure 2 shows the dependence of the critical acceleration for fluidization on the amount of helium gas added at different temperatures around the  $\lambda$  point. For clearer display we use a scaled critical acceleration for fluidization  $\Gamma^* = (\Gamma_c - \Gamma_{\text{dry}}) / \Gamma_{\text{dry}}$ .  $\Gamma_{\text{dry}}$ , the fluidization acceleration for a dry sample, is an average of  $\Gamma_c$  before it increases due to wetting.

Moreover, we scale the amount of helium added,  $n$ , by the amount of helium gas needed for the pressure in the cell to reach saturation,  $n_{\text{sat}}$ , by defining  $n^* = n / n_{\text{sat}}$ . For  $n^* < 1$ ,  $n^*$  can be treated as the fractional saturation of helium,  $P_c / P_0$ , in the cell, where  $P_c$  is the pressure in the cell and  $P_0$  the saturated vapor pressure, because most of the helium added stays in the vapor phase. For  $n^* > 1$ ,  $n^* - 1$  grows linearly with liquid content  $W$ , by which we denote the ratio of the volume of the wetting liquid and the total volume occupied by the sample. The data with largest  $n^*$  shown below correspond to a liquid content varying from 10% to 38% at different temperature.

Figure 2 shows that the behavior of  $\Gamma^*$  can be divided into three distinct regimes. In regime 1 the sample behaves the same as a dry granular medium; the scaled critical acceleration stays around zero. Adding helium in this regime leads to the increase of pressure in the cell and the formation of the first atomic layer of helium on the particles. This layer is, however, not mobile enough to form liquid bridges [27].

Regime 2 corresponds to the asperity wetting regime, where  $\Gamma^*$  increases monotonically with the amount of added helium. In this regime the helium film condensed on the

particle surface is thick enough to form small liquid bridges between the asperities of adjacent particles. With the increase of helium adsorbed, the number of small capillary bridges at the asperity level increases, which leads to a higher cohesive force between adjacent particles.

In regime 3, the amount of adsorbed helium is enough to fill the roughness on the grains, such that they appear as completely wet, perfect spheres to all further added liquid.  $\Gamma^*$  shown in Fig. 2, within experimental scattering, stays constant, in agreement with earlier experiments with other liquids at room temperature [21]. This independence from  $n^*$  comes from the fact that the capillary force is dominated by the curvature of the spheres instead of the volume of the liquid bridges. With the increase of  $n^*$ , capillary bridges will coalesce and form bigger liquid clusters, but  $\Gamma^*$  will not change due to the constant Laplace pressure imposed by the packing geometry [22].

It is regime 2 where the difference between superfluid and normal fluid wetting is significant. For superfluid wetting the sample enters regime 2 already at a fractional saturation of about 0.75, which is far below the 0.95 observed for normal fluid wetting. We interpret the increase of  $\Gamma^*$  to be due to the formation of bridges between asperities of neighboring spheres by the condensed unsaturated helium film. The amount of helium adsorbed can be described by the Frenkel-Hasley-Hill equation [33,34]; it is proportional to  $[-\ln(P_c/P_0)]^{-1/3}$  and therefore as shown above to  $[-\ln(n^*)]^{-1/3}$ .

Figure 3(a) shows that  $\Gamma^*$  increases linearly in regime 2 with the unsaturated helium film thickness, both above and below the  $\lambda$  point. This can be understood in the following

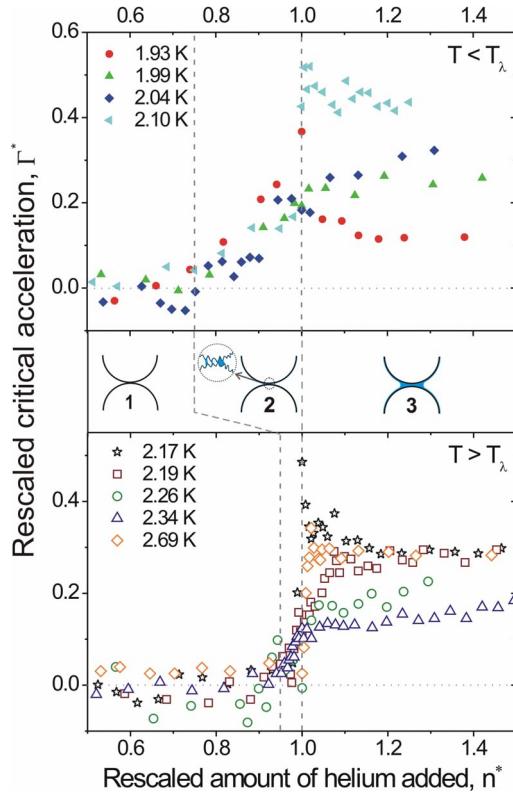


FIG. 2. (Color online) Scaled critical acceleration for fluidization,  $\Gamma^*$ , as a function of the amount of helium added,  $n^*$ , for superfluid (top) and normal fluid (bottom) wetting.  $\Gamma^*=0$  corresponds to the behavior of dry grains, and  $n^*=1$  to the transition from an unsaturated to a saturated helium film. Three different regimes can be distinguished: dry (1), asperity (roughness) (2), and complete wetting (3). Sketches of the three regimes on the grain size scale are shown in the middle. The dashed lines separating the regimes are guides to the eye. Each data point is an average of three measurements; the standard error is within 0.05.

way. To fluidize wet granular media, the driving force has to overcome the capillary forces between the grains or between container walls and the particles. The gravitational force can be neglected here because it is two orders of magnitude smaller than the capillary force. In the asperity regime 2, the capillary force  $f_b$  is given by [6]

$$f_b = \frac{R^2}{2\pi\delta^2} \tilde{V} F_b, \quad (1)$$

where

$$F_b = 2\pi R \gamma \cos(\theta) \quad (2)$$

is the capillary force in the complete wetting regime,  $R$  is the radius of the particle,  $\tilde{V}$  is the bridge volume, which depends linearly on the amount of helium adsorbed,  $\delta$  is the amplitude of the roughness of the particles, and  $\theta$  is the contact angle. The linear growth of the cohesive force with the bridge volume in this regime explains the linear dependence of  $\Gamma^*$  on the amount of helium adsorbed [Eq. (1)]. Therefore we fit in Fig. 3(a) the values of  $\Gamma^*$  with

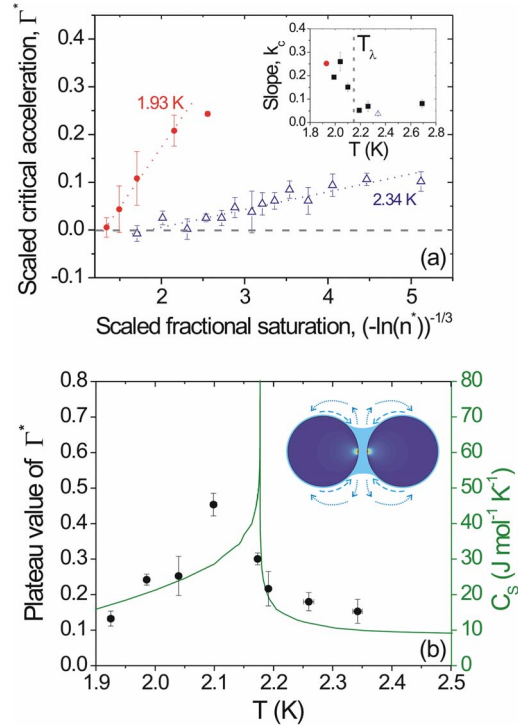


FIG. 3. (Color online) (a) In regime 2  $\Gamma^*$  varies linearly with the scaled saturation  $[-\ln(n^*)]^{-1/3}$ . Dotted lines are fits with Eq. (3). The inset of (a) shows the temperature dependence of the fit parameter  $k_c$ . (b) The temperature dependence of the plateau value of  $\Gamma^*$  in regime 3 (black dots). The dark green line is the specific heat  $C_s$  of bulk helium taken from [38]. The inset of (b) shows a sketch of two completely wetted particles. The color code illustrates the temperature gradients generated by energy dissipation. Blue dashed arrows indicate the flow of superfluid in the helium film driven by the fountain effect, and blue dotted arrows depict evaporation of helium from the surface of the meniscus.

$$\Gamma^* = k_c [-\ln(n^*)]^{-1/3} + \beta, \quad (3)$$

with the slope coefficient  $k_c$  and  $\beta$  as fitting parameters.

The temperature dependence of  $k_c$  shown in the inset of Fig. 3(a) depicts the enhancement of the cohesive force by adsorbed superfluid film below the  $\lambda$  point. This is readily explained from the strongly different transport mechanisms in the superfluid state. First, the superflow enables the forming capillary bridge to acquire more liquid from its surroundings during bridge formation. Second, the impact of the spheres radiates quantum excitations into the superfluid at the point of contact, dragging extra superfluid toward the contact region by osmosis (“fountain effect”) [28,29]. This is in contrast to normal fluid wetting, where only liquid very close to the contact point is sucked into the bridge by the negative Laplace pressure.

As is clearly seen in Fig. 2, the critical acceleration shows a plateau in regime 3 both above and below  $T_\lambda$ , as is observed as well with standard liquids [6,21,23]. The constancy of  $\Gamma^*$  reflects the weak dependence of the capillary force upon liquid volume for fully developed capillary bridges [6,22]. However, since the surface tension depends only weakly on temperature close to  $T_\lambda$ , we would expect to ob-

serve roughly the same plateau value for all temperatures, which is clearly not the case.

Figure 3(b) shows the temperature dependence of the plateau value of  $\Gamma^*$  in regime 3. It shows a peak at about 2.1 K, close to the superfluid transition. This can be qualitatively understood as a combination of two effects. In the normal fluid regime, capillary bridges will acquire their full volume only close to  $T_\lambda$ , where the specific heat of the liquid (shown for comparison) is large and prevents strong heating of the bridge from dissipated energy. Farther away from  $T_\lambda$ , the bridges heat up and evaporate back into the asperity regime. In the superfluid regime, temperature is effectively equalized by the superflow. The heat intake due to bridge rupture and grain impact thus gives rise to a strong superflow toward the contact points. However, it is well known that the presence of a superflow in an adsorbed liquid film leads to a strongly increased contact angle  $\theta$  [35]. This is due to the Kontorovich pressure term [36] adding to the disjoining pressure, and leads to dynamical incomplete wetting in liquid helium, as observed experimentally [37]. This effect is weak close to  $T_\lambda$ , but increases further into the superfluid regime. As a

consequence, the capillary force (and thus the plateau value of  $\Gamma^*$ ) is reduced according to Eq. (2).

We need to mention that no clear signature of a viscous effect can be found. This can be understood by calculating the ratio between the energy dissipation by viscosity and by rupture of capillary bridges [6]. At the temperature 2.1 K, it yields 0.0046, indicating that the system is still in the capillary region where viscosity can be ignored.

To conclude, we demonstrate with liquid helium, a liquid that has a surface tension only 1/200 that of pure water, that the increase of mechanical stability of granular materials by wetting is prominent. Beyond that, our main findings can still be explained on the basis of a simple capillary model [6] by taking superfluid properties of liquid helium, such as the “fountain effect”, into account.

Inspiring discussions with Mario Scheel, Axel Fingerle, Martin Brinkmann, Jürgen Vollmer, and Isaac Goldhirsch are gratefully acknowledged. We thank Udo Krafft and Günter von Roden for their indispensable technical support.

- 
- [1] J. Duran, *Sands, Powders, and Grains* (Springer, New York, 2000).
- [2] S. R. Nagel, *Rev. Mod. Phys.* **64**, 321 (1992).
- [3] D. J. Hornbaker, R. Albert, I. Albert, A.-L. Barabasi, and P. Schiffer, *Nature* (London) **387**, 765 (1997).
- [4] P. Schiffer, *Nat. Phys.* **1**, 21 (2005).
- [5] S. Nowak, A. Samadani, and A. Kudrolli, *Nat. Phys.* **1**, 50 (2005).
- [6] S. Herminghaus, *Adv. Phys.* **54**, 221 (2005), and references therein.
- [7] L. Bocquet, E. Charlaix, S. Ciliberto, and J. Crassous, *Nature* (London) **396**, 735 (1998).
- [8] L. Bocquet, É. Charlaix, and F. Restagno, *C. R. Phys.* **3**, 207 (2002).
- [9] T. C. Halsey and A. J. Levine, *Phys. Rev. Lett.* **80**, 3141 (1998).
- [10] W. B. Pietsch, *Nature* (London) **217**, 736 (1968).
- [11] Th. Brunet, X. Jia, and P. Mills, *Phys. Rev. Lett.* **101**, 138001 (2008).
- [12] H. Rumpf, *Agglomeration* (AIME Interscience, New York, 1962).
- [13] S. M. Iveson, J. D. Litster, K. Hapgood, and B. J. Ennis, *Powder Technol.* **117**, 3 (2001).
- [14] T. Gröger, U. Tüzün, and D. M. Heyes, *Powder Technol.* **133**, 203 (2003).
- [15] A. Fingerle, K. Roeller, K. Huang, and S. Herminghaus, *New J. Phys.* **10**, 053020 (2008).
- [16] I. Gutman, *Industrial Uses of Mechanical Vibrations* (Business Books, London, 1968).
- [17] A. Alexeev, V. Royzen, V. Dudko, A. Goldshtein, and M. Shapiro, *Phys. Rev. E* **59**, 3231 (1999).
- [18] A. Götzenoder, C.-H. Tai, C. A. Kruelle, I. Rehberg, and S.-S. Hsiau, *Phys. Rev. E* **74**, 011304 (2006).
- [19] N. Mujica and F. Melo, *Phys. Rev. Lett.* **80**, 5121 (1998).
- [20] J. S. Olafsen and J. S. Urbach, *Phys. Rev. Lett.* **95**, 098002 (2005).
- [21] M. Scheel, D. Geromichalos, and S. Herminghaus, *J. Phys.: Condens. Matter* **16**, S4213 (2004).
- [22] M. Scheel, R. Seemann, M. Brinkmann, M. Di Michiel, A. Sheppard, B. Breidenbach, and S. Herminghaus, *Nature Mater.* **7**, 189 (2008).
- [23] Z. Fournier *et al.*, *J. Phys.: Condens. Matter* **17**, S477 (2005).
- [24] E. Cheng, M. W. Cole, W. F. Saam, and J. Treiner, *Phys. Rev. Lett.* **67**, 1007 (1991).
- [25] J. Klier, P. Stefanyi, and A. F. G. Wyatt, *Phys. Rev. Lett.* **75**, 3709 (1995).
- [26] N. Bigelow, P. J. Nacher, and J. Dupont-Roc, *J. Low Temp. Phys.* **89**, 135 (1992).
- [27] J. Wilks, *The Properties of Liquid and Solid Helium* (Clarendon Press, Oxford, 1967).
- [28] J. F. Allen and H. Jones, *Nature* (London) **141**, 243 (1938).
- [29] H. London, *Proc. R. Soc. London, Ser. A* **171**, 484 (1939).
- [30] E. Long and L. Meyer, *Phys. Rev.* **85**, 1030 (1952).
- [31] L. Meyer, *J. Low Temp. Phys.* **3**, 199 (1970).
- [32] K. R. Atkins, B. Rosenbaum, and H. Seki, *Phys. Rev.* **113**, 751 (1959).
- [33] R. Bowers, *Philos. Mag.* **44**, 485 (1953).
- [34] J. Israelachvili, *Intermolecular and Surface Forces* (Academic, San Diego, 1992).
- [35] S. Herminghaus, *Europhys. Lett.* **42**, 443 (1998).
- [36] V. M. Kontorovich, *Sov. Phys. JETP* **3**, 770 (1956).
- [37] M. Poujade, C. Guthmann, and E. Rolley, *Europhys. Lett.* **58**, 837 (2002).
- [38] R. J. Donnelly and C. F. Barenghi, *J. Phys. Chem. Ref. Data* **27**, 1217 (1998).